Sintering reaction and microstructure of MAl (M = Ni, Fe, and Mg) nanoparticles through molecular dynamics simulation*

Yuwen Zhang(张宇文)[1], Yonghe Deng(邓永和)[2,†], Qingfeng Zeng(曾庆丰)[3], Dadong Wen(文大东)[2], Heping Zhao(赵鹤平)[1], Ming Gao(高明)[1], Xiongying Dai(戴雄英)[2], and Anru Wu(吴安如)[4]

[1] *College of Physics, Mechanical and Electrical Engineering, Jishou University, Jishou* 416000, *China*
[2] *School of Computational Science and Electronics, Hunan Institute of Engineering, Xiangtan* 411104, *China*
[3] *School of Physics, Guizhou University, Guiyang* 550025, *China*
[4] *Hunan Provincial Key Laboratory of Vehicle Power and Transmission Systems, Hunan Institute of Engineering, Xiangtan* 411104, *China*

(Received 8 May 2020; revised manuscript received 1 July 2020; accepted manuscript online 6 July 2020)

The sintering–alloying processes of nickel (Ni), iron (Fe), and magnesium (Mg) with aluminum (Al) nanoparticles were studied by molecular dynamics simulation with the analytic embedded-atom model (AEAM) potential. Potential energy, mean heterogeneous coordination number $N_{\mathrm{A}}^{\mathrm{B}}$, and surface atomic number $N_{\mathrm{surf-A}}$ were used to monitor the sintering–reaction processes. The effects of surface segregation, heat of formation, and melting point on the sintering–alloying processes were discussed. Results revealed that sintering proceeded in two stages. First, atoms with low surface energy diffused onto the surface of atoms with high surface energy; second, metal atoms diffused with one another with increased system temperature to a threshold value. Under the same initial conditions, the sintering reaction rate of the three systems increased in the order MgAl < FeAl < NiAl. Depending on the initial reaction temperature, the final core–shell (FeAl and MgAl) and alloyed (NiAl and FeAl) nanoconfigurations can be observed.

Keywords: molecular dynamics, AEAM potential, core–shell structure, sintering, nanoparticles

PACS: 66.30.Pa, 75.75.Jn, 73.63.Bd, 78.67.Bf **DOI:** 10.1088/1674-1056/aba2dd

1. Introduction

The physical and chemical properties of metal clusters significantly differ from those of their corresponding bulk materials.[1,2] Considering the synergistic effects among metals, bimetallic nanoclusters are eliciting more research interest than monometallic ones.[3,4] Generally, the physical and chemical properties of binary metal clusters can be altered by varying their composition, atomic distribution, and structure,[5,6] enabling potential applications such as in catalysis fuel cells and hydrogen storage.[7]

The structure types of bimetallic nanoalloys primarily include mixed structure, segregation structure, core–shell structure, and onion-like three-layer structure.[4] However, the microscopic mechanism of nanoalloy-structure formation is difficult to observe through experiments. Molecular dynamics (MD) simulation can offer insights into this process at the atomic scale.

MD simulations of metal–cluster collision, coalescence, and sintering reaction have been extensively performed.[1,8–17] Marcelo *et al.* reported core–shell (PtAu), alloyed (PdAu), and onion-like (CuAg) cluster structures by colliding two different metal clusters at various initial velocities.[3] Yang *et al.* simulated the sintering reaction between Li and Pd metal clusters at different initial temperatures[8] and found that metal nanoclusters may undergo structural transformation during collision and coalescence,[1,18,19] Grammatikopoulos *et al.* conducted a classical MD simulation of palladium (Pd) clusters' coalescence and performed magnetron sputtering of inert gas for the condensation deposition of Pd nanoparticles.[19] They found that Pd atomic rearrangements triggered a crystallization wave propagating through the amorphous nanoparticles, forming mono- or polycrystalline face-centered cubic (FCC) structures.

Considerable theoretical studies have focused on sintering reactions among nanoparticles, but little attention has been paid to the differences in sintering reactions among different materials. NiAl nanoparticles, which possess high energy density and good mechanical properties at elevated temperatures, are considered as important materials.[20] Synthesized FeAl nanoparticles possess ferromagnetism above room temperature compared with their corresponding bulk crystalline materials that are nonmagnetic.[21] MgAl alloys are corrosion resistant and highly wieldable, and adding up to 10% of Mg to Al increases its strength while retaining its low density.[22,23] In the present work, we studied the sintering reaction between M (M = Ni, Fe, and Mg) cluster and Al cluster through MD simulation with the analytic embedded-atom model (AEAM) potential.[7] A comparative study of the three systems can reveal the dependence of sintering reaction on heat formation,

*Project supported by the National Natural Science Foundation of China (Grant Nos. 11572124 and 51871096) and the Natural Science Foundation of Hunan Province of China (Grant Nos. 2018JJ4044 and 2018JJ3100).
†Corresponding author. E-mail: dengyonghe1@163.com
© 2020 Chinese Physical Society and IOP Publishing Ltd

surface energy, and nanocluster melting point. Behavior differences in sintering reaction among the three systems were reasonably explained by surface segregation, heat formation, and melting point.

2. Simulation details

The sintering–alloying processes of M (M = Ni, Fe, and Mg) with Al nanoparticles were studied by MD simulations. The cluster size (N) of an icosahedron (ICO) structure with closed shells can be written as follows:[24]

$$N_l = \frac{10}{3}l^3 + 5l^2 + \frac{11}{3}l + 1, \tag{1}$$

where, l is the shell number in the ICO cluster. A typical ICO nanoparticle model contains 20 {111} facets, 30 edges, and 12 vertices. A three-mark ICO[25] containing 147, 309, and 561 atoms were built as the initial configurations of NiAl, FeAl, and MgAl nanoparticles (see Fig. 1). A realistic interatomic potential with AEAM formalism was used. The AEAM potential had been proven effective in describing NiAl,[20,26] FeAl,[27,28] and MgAl[29,30] nanoparticles and successfully been applied to study the bulk, surface, and clusters of metals and alloys. To check the validity of AEAM in the three systems, the heats of formation (ΔH) for the three possible intermetallics M_3Al (L12), MAl (B2), and MAl$_3$ (L12) and surface energies of the four metals were determined and are listed in Tables 1 and 2. The ΔH values were consistent reasonably with first-principle calculations.[23,31] The calculated surface energies were consistently lower than the first-principle calculations and experimental values for two reasons. First, given that the embedding functions of AEAM are too flat, it generally tends to underestimate the surface energy.[32] Second, the materials for experiments always have some defects that may lead a large surface energy. Notably, the present AEAM obtained the correct order of surface energy. The close-packed (111) face had the lowest surface energy, followed by the (100) and (110) faces for Ni and Al with FCC arrangement, respectively. For BCC arrangement, Fe (110) had the lowest surface energy. The order was particularly important for studying surface segregation and nanoalloys configurations.[33,34] Accordingly, the present NiAl, FeAl, and MgAl alloying potential can be used for wide-ranging components with reasonable accuracy. In general, the ΔH of a system with a given structure can be written in the form[35]

$$\Delta H = [E(\mathrm{A}_n\mathrm{B}_m) - nE_\mathrm{A} - mE_\mathrm{B}]/(n+m). \tag{2}$$

Here, n and m are the number of A and B atoms in the system, respectively; E ($\mathrm{A}_n\mathrm{B}_m$) is the total energy of the intermetallic $\mathrm{A}_n\mathrm{B}_m$; and E_A and E_B are the cohesive energy of the A and B atoms, respectively. If the ΔH of a system is negative, it would easily form alloys, which helps reduce the energy of the system; otherwise, it would easily form a phase-segregated structure.[36,37] Surface energy, defined as the excess free energy on the surface of a specific crystal plane per unit area, is a basic physical quantity in surface physics. It determines the equilibrium form of a crystal and plays an important role in crystal formation, coarsening, and growth.[38] The calculated expression is as follows:[39]

$$E_\mathrm{surf} = (E_\mathrm{A} - E_\mathrm{bulk})/S, \tag{3}$$

where E_A is the total energy when the system is a free surface, S is the surface area of the free surface of the system, and E_bulk is the total energy of the system under periodic conditions.

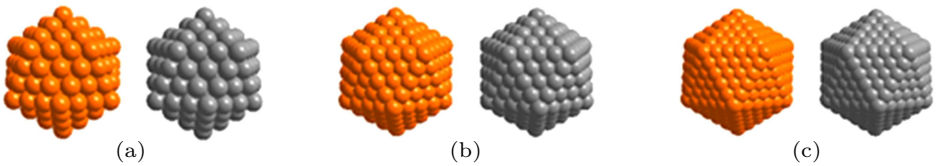


Fig. 1. Initial configuration of different particles. (a) $M_{147}\mathrm{Al}_{147}$ nanoparticles; (b) $M_{309}\mathrm{Al}_{309}$ nanoparticles; (c) $M_{561}\mathrm{Al}_{561}$ nanoparticles. M (M = Mg, Ni, and Fe) and Al atoms are shown as orange and gray spheres, respectively.

Table 1. The heats of formation (ΔH) for M_3Al, MAl, and MAl$_3$ (M = Ni, Fe, and Mg).

Material	Structure	ΔH/(eV/atom)	
		Present	The first principles calculations
MgAl	B2	–0.024	0.051[23]
$MgAl_3$	L12	–0.031	–0.015[23]
Mg_3Al	L12	–0.007	–0.005[23]
NiAl	B2	–0.66	–0.67[31]
$NiAl_3$	L12	–0.27	
Ni_3Al	L12	–0.52	–0.44[31]
FeAl	B2	–0.27	–0.28[23]
$FeAl_3$	L12	–0.045	–0.11[23]
Fe_3Al	L12	–0.17	–0.19[23]

The Nose–Hoover thermostat was used to control the temperature of the system during the heating processes of the single M (M = Ni, Fe, and Mg) and Al nanoparticles. The microcanonical ensemble was utilized to simulate the sintering reaction of M with Al nanoparticles. Before sintering, the two nanoparticles that were relaxed at 0 K were heated to the specified temperature, and then the equilibrium position was extracted as the initial configuration of the sintering reaction. In the sintering simulation, the single M (M = Ni, Fe, and Mg) and Al nanoparticles were separated along the x axis at an appropriate interval, which was within the cutoff distance of the interaction potential of M and Al elements.[7]

Table 2. The surface energy (E_{surf}) and atomic radius (r_{atom}) for Ni, Fe, Mg, and Al with different structures and surfaces, the first principle (FP) calculations[38] as well as available theory value[7] (EMP) are also listed.

Material	Structure	E_{surf}/(mJ/m^2)			r_{atom}/nm
		Surface	Present	FP	EMP
Ni	FCC	(111)	1749	2011	0.1243
		(110)	1935	2368	
		(100)	1793	2426	
Fe	BCC	(111)	1510	2733	0.1124
		(110)	1230	2430	
		(100)	1356	2222	
Mg	HCP	(0001)	301	792	0.1590
Al	FCC	(111)	713	939	0.1426
		(100)	747	1081	
		(110)	809	1090	

Equations of motion were integrated by a fifth-order gear predictor–corrector algorithm[40] with an appropriate time step $\Delta t = 0.5$ fs. During sintering, the alloying process of the system was characterized by calculating the evolution of temperature, surface atomic number, and heterogeneous coordination number with time.[8]

3. Results and discussion

3.1. Melting point of single nanoparticles

The melting of single Ni, Fe, Mg, and Al nanoparticles containing different atoms were studied. In the initial heating stage of the nanoparticles, the corresponding temperature increment was 50 K. However, a smaller step of 10 K was adopted to determine the melting point more accurately with increased temperature up to around the melting point.[41] The evolution of the potential energy (PE) per atom with temperature is shown in Fig. 2.

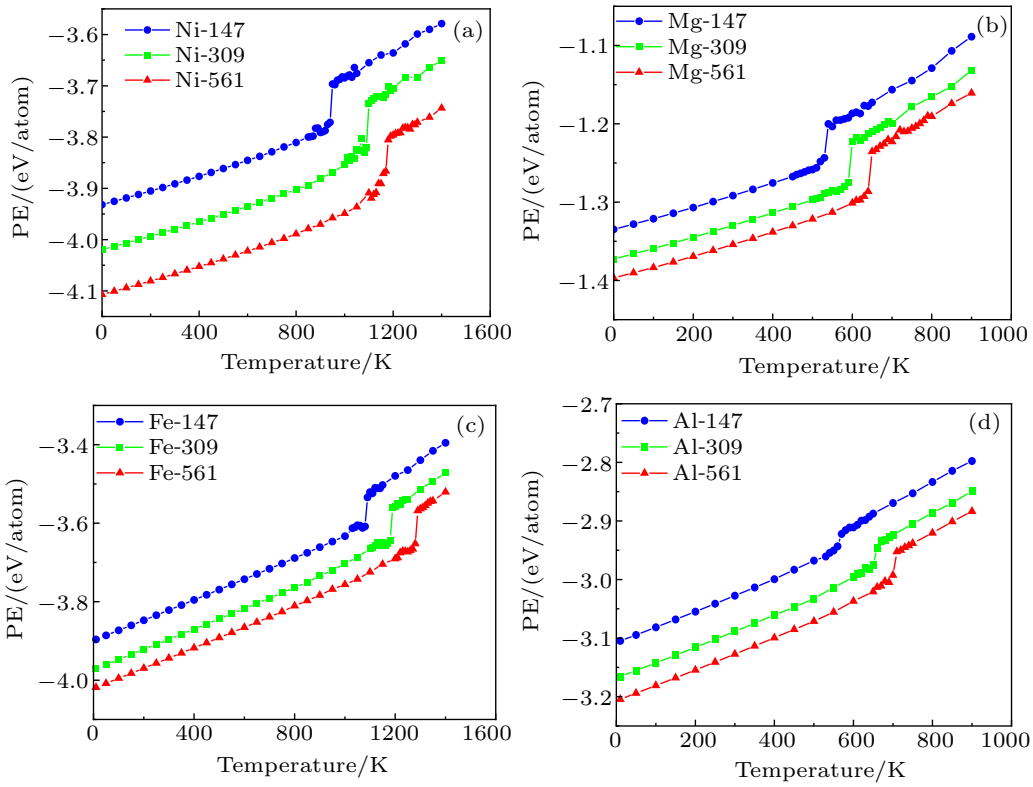


Fig. 2. The evolution of the potential energy (PE) per atom with temperature for pure Ni (a), Mg (b), Fe (c), and Al (d) nanoparticles with ICO configuration.

Notably, PE for each nanoparticle initially increased linearly with temperature. With further increased temperature, a sudden jump in the PE curve of each nanoparticle was observed because of the latent heat of melting.[42] Therefore, we defined the temperature of the jump point as the melting point of the nanoparticle. The melting point increased with increased atom number in the nanoparticles for each metal. This finding was similar to some previous ones in that the melting point of particles increases with increased size, finally approaching those of the corresponding bulk materials.[13,43–45] This phenomenon may result from the increased proportion of surface atoms with decreased particle size. Surface atoms are known to have fewer coordination numbers than bulk atoms and thus have higher energies. For the same number of atoms, the melting points of Ni and Fe nanoparticles were higher than those of Mg and Al nanoparticles. This finding can be attributed to the cohesion energy of metal Ni (−4.45 eV/atom) and metal Fe (−4.28 eV/atom) being much lower than those of metal Al (−3.39 eV/atom), and metal Mg (−1.51 eV/atom).[23,46–49] The melting points for all single nanoparticles are listed in Table 3.

Table 3. Melting point for single Ni, Fe, Mg, and Al nanoparticle with sizes ($N = 147$, 309, and 561).

Material	Melting point/K		
	$N = 147$	$N = 309$	$N = 561$
Ni	950	1100	1180
Fe	1090	1190	1290
Al	570	660	710
Mg	540	600	650

3.2. Sintering–alloying of nanoparticles

3.2.1. Evolution of temperature

The effects of size ($N = 147$, 309, and 561) and initial temperature on the sintering reaction of M ($M =$ Ni, Fe, and Mg) with Al nanoparticles were examined. We found that nanoparticle size had no obvious effect on the results. Hence, the initial temperature dependence of the sintering reactions of $Fe_{309}Al_{309}$, $Mg_{309}Al_{309}$, and $Ni_{561}Al_{561}$ nanoparticles was discussed.

The temperature evolution of the $Fe_{309}Al_{309}$, $Mg_{309}Al_{309}$, and $Ni_{561}Al_{561}$ nanoparticles with reaction time at different initial temperatures during sintering under adiabatic condition is shown in Fig. 3. The temperature of the systems rose faster at higher initial temperature T_{init}. As shown in Fig. 3(a), the temperature of $Fe_{309}Al_{309}$ nanoparticles almost remained constant during the reaction when $T_{init} < 300$ K. Two stages were observed in the T–t curve of the $Fe_{309}Al_{309}$ system when T_{init} reached 300 K. The sudden jump of the temperature at a very early time was due to the release of the system surface energy after Fe_{309} and Al_{309} nanoparticles made contact. The following gradual increase in temperature indicated increased number of FeAl hetero-coordination. When T_{init} was above 400 K, three stages were observed in the T–t curve. At the beginning of the contact between the two nanoparticles, the temperature of the system rose rapidly and then remained constant at the first stage. The temperature of the system then rose again and reached a stable value at the second stage. At third stage when $T_{init} > 300$ K, the temperature of the system rose rapidly in a short time before reaching a stable value. As for $Mg_{309}Al_{309}$ nanoparticles, only two stages were observed, and the trend was gradual ascension with prolonged reaction time, as shown in Fig. 3(b). By contrast, when the sintering reaction of $Ni_{561}Al_{561}$ nanoparticles occurred in only hundreds of picoseconds, the temperature increased much faster than it did in the $Fe_{309}Al_{309}$ and $Mg_{309}Al_{309}$ systems, as shown in Fig. 3(c). The calculated ΔH values for the resulting MAl ($M =$ Ni, Fe, and Mg) nanoparticles with different sizes are shown in Fig. 4. The differences may be attributed mostly to the ΔH of NiAl being much more negative than those of FeAl and MgAl, and to the heat released by the FeAl and NiAl systems being much higher than that of MgAl. Experiments and theoretical studies showed that ΔH decreased in the order NiAl > FeAl > MgAl, and that the alloying capability of NiAl was the strongest, followed by those of FeAl and MgAl (a weakly miscible system).[23,50,51]

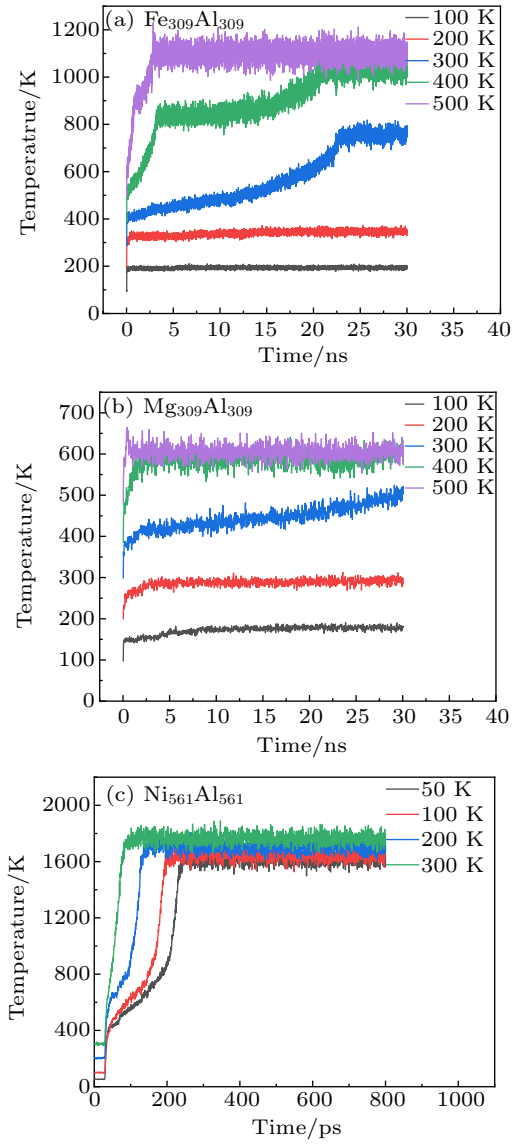


Fig. 3. The temperature evolution of the $Fe_{309}Al_{309}$, $Mg_{309}Al_{309}$, and $Ni_{561}Al_{561}$ nanoparticles with relation time at different initial temperatures.

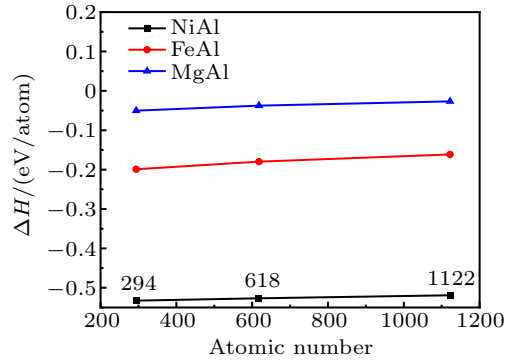


Fig. 4. Heats of formation for resulting MAl ($M =$ Ni, Fe, and Mg) nanoparticles with the size of the atom.

3.2.2. Configuration of nanoparticles

The final configurations of MAl ($M =$ Ni, Fe, and Mg) nanoparticles were examined to further understand the effect of initial temperature (T_{init}) on the alloying reaction processes.

Figure 5(a) illustrated the final configuration of $Fe_{309}Al_{309}$ nanoparticles and their cross-sections at different T_{init} values. Interestingly, a well-defined core–shell FeAl nanoparticle without the penetration of Al into the Fe core can be formed at $T_{init} = 300$ K. By contrast, an alloyed Fe/Al nanoparticle with Al atoms enriched on the surface of the nanoclusters formed at $T_{init} = 400$ K. As for initial temperatures much lower than 300 K, *e.g.*, $T_{init} = 200$ K, the FeAl nanoparticle was not fully fused and formed a neck similar to previous findings.[10,52,53] These different final configurations may have resulted from the following. At a low initial temperature, although the merging nanoparticles released considerable surface energy to increase the temperature of the system, the released energy was not sufficiently high to make the Al atoms spread completely across the surface of Fe cores. When the T_{init} approached 300 K, the released surface energy can make the Al atoms gradually cover the Fe core. Due to the higher melting point of Fe nanoparticles and the insufficient temperature of the system, Al atoms were unable to enter the Fe core to diffuse with it. When T_{init} exceeded a threshold value, the merging nanoparticles released sufficient energy to make the Fe and Al atoms diffuse with each other, thereby reducing the PE of the system and accelerating the alloying process of the system.

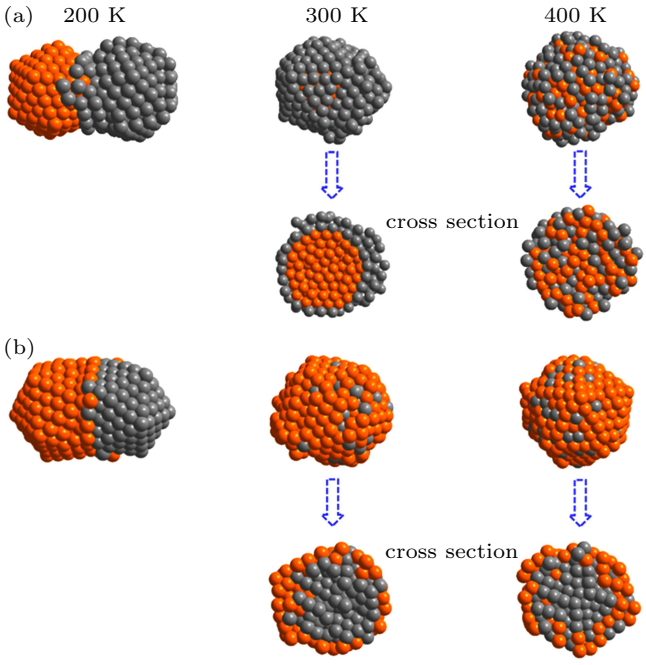


Fig. 5. Final configurations of $M_{309}Al_{309}$ (M = Fe and Mg) nanoparticles after sintering for three different initial temperatures. (a) $Fe_{309}Al_{309}$; (b) $Mg_{309}Al_{309}$. The orange and gray balls represent M (M = Fe and Mg) and Al atoms, respectively.

The final configurations of $Mg_{309}Al_{309}$ nanoparticles for the three different initial temperatures are shown in Fig. 5(b). Similar to $Fe_{309}Al_{309}$ particles, ICO $Al_{core}Mg_{shell}$ configurations were also observed for $T_{init} = 300$ K and 400 K. In the ICO $Al_{core}Mg_{shell}$ nanoparticles, Mg shells contained a small number of Al atoms, and the proportion of Al atoms increased with increased T_{init}. These phenomena may have resulted from the fact that Mg atom possessed a smaller surface energy and a larger atomic radius than Al atom, tending to occupy the surface of nanoparticles.[4,7,54] Instead of core–shell configurations, only alloyed $Ni_{561}Al_{561}$ nanoparticles were observed for various initial temperatures. The three stages of sintering of $Ni_{561}Al_{561}$ nanoparticles at $T_{init} = 100$ K are shown in Fig. 6. The collision point[52] can be observed in Fig. 6(a). As discussed above, the decrease in the total surface of the system may have led to the rapid decrease in PE. The surface diffusion stage of Al atoms on the Ni cores is shown in Fig. 6(b), and the configuration after 300 ps is depicted in Fig. 6(c). Roughly spherical NiAl alloyed clusters were observed. Given that Al atoms have a smaller surface energy and a larger atomic radius than Ni atoms,[7] we also observed that Al atoms were enriched on the surface of the nanoclusters. In general, the segregation of atoms with large atomic radii from the bulk to the surface decreases the atomic-mismatch elastic energy, and internal stress can be released this way.[43] Furthermore, atoms with small surface energies enriched on the surface are favorable for reducing the surface energy of nanoparticles.[36] The surface energies and atomic radius of M (M = Ni, Fe, and Mg) and Al atoms are listed in Table 2.

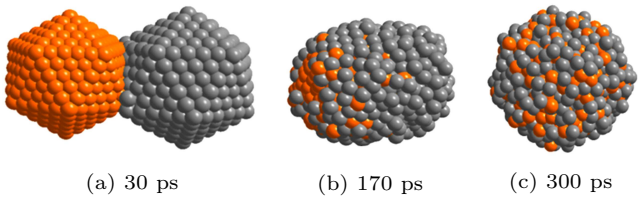


Fig. 6. The evolution of $Ni_{561}Al_{561}$ nanoparticle at $T_{init} = 100$ K. (a) Collision point; (b) diffusion stage; (c) final configuration. The orange and gray balls represent Ni and Al atoms, respectively.

3.2.3. Path of sintering reaction

The sintering–alloying processes were further characterized using the mean heterogeneous coordination number N_A^B (*i.e.*, the average atomic coordination number of B-type atoms around A-type atoms) and the surface atomic number N_{surf-A} (*i.e.*, the number of surface atoms of A-type atoms).[8] The N_{surf-A} of MAl nanoparticles as a function of relaxation time at different T_{init} values is shown in Fig. 7. At the initial temperature of 300 K, the $N_{surf-Fe}$ of $Fe_{309}Al_{309}$ nanoparticles remained constant for about 12 ns and then decreased rapidly to zero, thereafter remaining unchanged. However, at $T_{init} = 400$ K and 500 K, $N_{surf-Fe}$ decreased sharply to zero and then increased to a stable value. This finding indicated that with the relaxation at $T_{init} > 300$ K, Al atoms gradually covered the Fe core, and then the Fe and Al atoms began to diffuse with each other to further increase the temperature of the system, resulting in alloyed $Fe_{309}Al_{309}$ nanoparticles.

The time evolution of N_{surf-A} of $Mg_{309}Al_{309}$ nanoparticles was similar to that of $Fe_{309}Al_{309}$ nanoparticles but very different from that of $Ni_{561}Al_{561}$ nanoparticles. For $Ni_{561}Al_{561}$ nanoparticles, N_{surf-A} decreased rapidly to a minimum then

increased to a critical value. With increased $T_{\rm init}$, given that the NiAl system had better alloying ability than the FeAl and MgAl systems,[7] the minimum of $N_{\rm surf-A}$ increased evidently. During the reaction of $Ni_{561}Al_{561}$, the temperature of the system rose sufficiently high before the Al atoms completely covered the surface of the Ni core. In this case, the Ni and Al atoms had begun to diffuse with each other, further releasing the PE of the system and increasing its temperature to accelerate diffusion. The evolution of the mean heterogeneous coordination number $N_{\rm A}^{\rm B}$ showed similar results to the $N_{\rm surf-A}$reflected for each system. As shown in Fig. 8, for MAl (M = Ni, Fe, and Mg) nanoparticles, the evolution trend of $N_{\rm A}^{\rm B}$ with time well agreed with the evolution trend of system temperature with time (Fig. 3).

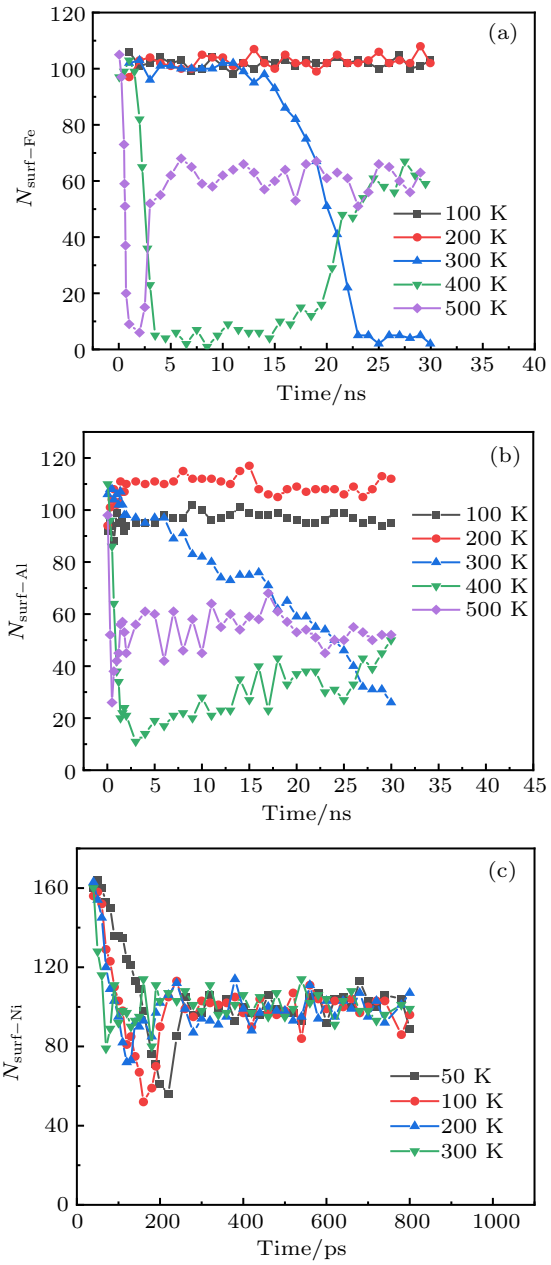


Fig. 7. Time evolution with the surface atomic number $N_{\rm surf}$ in MAl (M = Fe and Mg) nanoparticles for the various initial temperatures. (a) $Fe_{309}Al_{309}$, (b)$Mg_{309}Al_{309}$, (c) $Ni_{561}Al_{561}$.

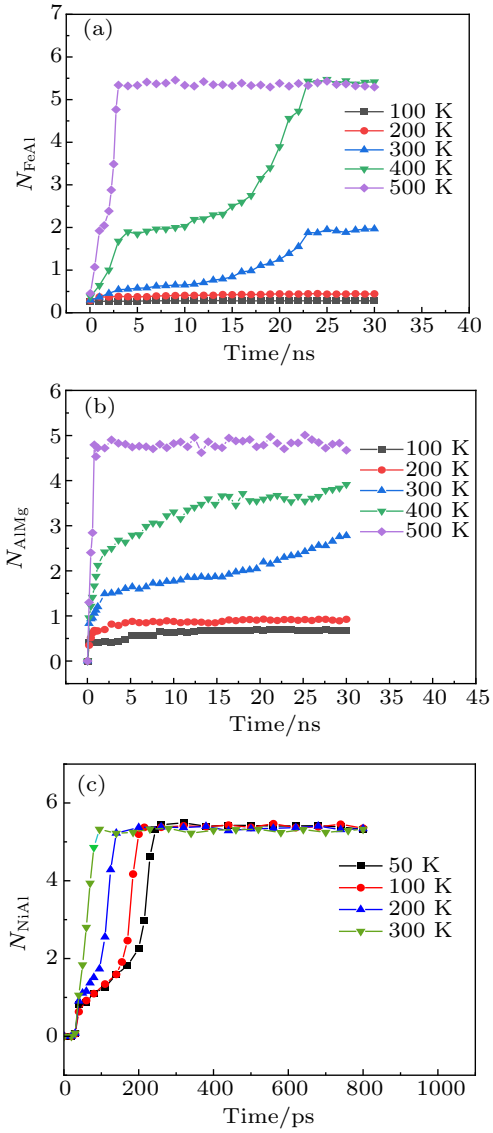


Fig. 8. The evolution trend of $N_{\rm A}^{\rm B}$ of MAl (M = Ni, Fe, and Mg) nanoparticles with time for different initial temperatures during the sintering. (a) $Fe_{309}Al_{309}$; (b) $Mg_{309}Al_{309}$; (c) $Ni_{561}Al_{561}$.

According to the evolution of $N_{\rm A}^{\rm B}$ and $N_{\rm surf-A}$ with time, the three systems had similar sintering reaction paths. The metal with a lower surface energy first gradually diffused to cover the core substrate with a higher surface energy. For the FeAl system, Al shell and Fe core atoms diffused with each other when $T_{\rm init}$ exceeded a certain critical value. For the NiAl system, Al and Ni atoms began to diffuse with each other before Al atoms completely covered the Ni core substrate. For the MgAl system, Al atoms and Mg atoms hardly diffused with each other after forming the $Mg_{\rm shell}Al_{\rm core}$ structure.

3.3. Effects of surface segregation, alloying, and melting point on sintering

The effects of surface segregation, alloying, and melting point of nanoparticles on the sintering of the MAl (M = Ni, Fe, and Mg) systems were discussed. As mentioned above, the final structure of the NiAl system was alloyed, but that of the FeAl system depended on the $T_{\rm init}$ of sintering. By contrast,

at $T_{\text{init}} > 300$ K, the final configuration of the MgAl system was the $\text{Al}_{\text{core}}\text{Mg}_{\text{shell}}$ structure. As shown in Fig. 4, the NiAl system had a more negative ΔH than the other two systems. The melting point of Ni was also much higher than that of Al nanoparticles with the same number of atoms. As a result, the alloying ability of NiAl was stronger than the surface segregation of Al in the sintering reaction.

However, due to the moderate ΔH of FeAl nanoparticles compared with those of NiAl and MgAl nanoparticles, as well as the much higher melting point of Fe than Al, the heat released by the collision of Fe and Al was insufficient to induce FeAl alloying at a low initial temperature. Hence, the $\text{Fe}_{\text{core}}\text{Al}_{\text{shell}}$ structure was formed. For MgAl nanoparticles, because ΔH was almost equal to zero, the melting point of Mg and Al was very close and indicated a weak miscible system. Considering the much lower surface energy of Mg than Al, the $\text{Al}_{\text{core}}\text{Mg}_{\text{shell}}$ structure was observed in the sintering reaction. Therefore, alloying and surface segregation in the sintering process affected the final configuration of nanoparticles. In the NiAl system, alloying effect played a crucial role in sintering. For the FeAl system, Al surface segregation and alloying were pronounced, and the final nanoparticle configuration depended mostly on the initial reaction temperature. However, the surface segregation of Mg atoms dominated the sintering reaction of MgAl nanoparticles.

4. Conclusions

The sintering–alloying processes of Ni, Fe, and Mg with Al nanoparticles at different temperatures were investigated by MD simulations with the AEAM potential. Several methods were used to analyze the reaction processes, and results showed that sintering proceeded in two stages. First, atoms with low surface energies diffused on the surface of atoms with high surface energies. Second, metal atoms diffuse with each other after the system temperature was increased to a threshold value.

Under the same initial conditions, the sintering reaction rate of the three systems increased in the order MgAl < FeAl < NiAl. The final core–shell (FeAl and MgAl) and alloyed (NiAl and FeAl) nanoconfigurations strongly depended on the initial reaction temperature. The reaction processes of the nanoalloys were determined by the ΔH of the system, the surface energy of the metal, and the melting point of nanoparticles.

References

[1] Antunez-Garcia J, Mejia-Rosales S, Perez-Tijerina E, Montejano-Carrizales J M and Jose-Yacaman M 2011 *Materials (Basel)* **4** 368
[2] Songül Taran A K G and Haydar Arslan 2020 *Chin. Phys. B* **29** 077801
[3] Dassie S A and Leiva E P 2005 *J. Chem. Phys.* **123** 184505
[4] Riccardo F, Julius J and Johnston R L 2008 *Chem. Rev.* **108** 845
[5] Li G, Wang Q, Liu T, Wang K and He J 2010 *J. Cluster Sci.* **21** 45
[6] Jian H H, Bao D L, Zhang Y Y and Du S X 2020 *Chin. Phys. B* **29** 048701
[7] Yang J Y, Hu W Y, Wu Y R and Dai X Y 2012 *Surf. Sci.* **606** 971
[8] Yang L Y, Gan X L, Xu C, Lang L, Jian Z Y, Xiao S F, Deng H Q, Li X F, Tian Z A and Hu W Y 2019 *Comput. Mater. Sci.* **156** 47
[9] Li M, Hou Q and Wang J 2017 *Nucl. Instrum. Methods Phys. Res. B* **410** 171
[10] Arcidiacono S, Bieri N R, Poulikakos D and Grigoropoulos C P 2004 *Int. J. Multiph. Flow* **30** 979
[11] Moitra A, Kim S, Kim S-G, Park S J, German R M and Horstemeyer M F 2010 *Acta Mater.* **58** 3939
[12] Ma B, Zeng H, Cheng X, Zhang C and Lu Z 2019 *Comput. Mater. Sci.* **163** 167
[13] Ding F, Rosén A and Bolton K 2004 *Phys. Rev. B* **70** 075416
[14] Liu C M, Xu C, Cheng Y, Chen X R and Cai L C 2013 *Phys. Chem. Chem. Phys.* **15** 14069
[15] Guevara-Chapa E and Mejía-Rosales S 2014 *J. Nanopart. Res.* **16** 2757
[16] Henz B J, Hawa T and Zachariah M 2009 *Mol. Simul* **35** 804
[17] Zheng Q Y, Li Y, Wu W J, Shi M M, Yang B B and Zou J 2019 *Chin. Phys. B* **28** 108102
[18] Kim H Y, Lee S H, Kim H G, Ryu J H and Lee H M 2007 *Mater. Trans.* **48** 455
[19] Grammatikopoulos P, Cassidy C, Singh V and Sowwan M 2014 *Sci. Rep.* **4** 5779
[20] Tang J and Yang J 2013 *Thin Solid Films* **536** 318
[21] Pithawalla Y B, El-Shall M S and Deevi S C 2001 *J. Phys. Chem. B* **105** 2085
[22] Narasimhan S and Davenport J W 1995 *Phys. Rev. B* **51** 659
[23] Jelinek B, Groh S, Horstemeyer M F, Houze J, Kim S G, Wagner G J, Moitra A and Baskes M I 2012 *Phys. Rev. B* **85** 245102
[24] Martin T P 1996 *Phys. Rep.* **273** 199
[25] Schebarchov D and Hendy S C 2005 *Phys. Rev. Lett.* **95** 116101
[26] Tang J F and Yang J Y 2013 *J. Nanopart. Res.* **15** 2050
[27] Yang J Y, Hu W Y and Tang J F 2013 *RSC Adv.* **4** 2155
[28] Yang J Y, Hu W Y, Tang J F and Dai X Y 2013 *Comput. Mater. Sci.* **74** 160
[29] Dai X Y, Hu W Y, Yang J Y and Yi G J 2017 *Thin Solid Films* **626** 178
[30] Dai X Y, Hu W Y, Yang J Y and Chen C P 2015 *Physica B: Condens. Matter* **458** 144
[31] Wang Y, Liu Z K and Chen L Q 2004 *Acta Mater.* **52** 2665
[32] Haftel M 1993 *Phys. Rev. B* **48** 2611
[33] Los J, Mottet C and Tréglia G 2013 *Phys. Rev. B* **88** 165408
[34] Yun K Y, Cho Y H, Cha P R, Lee J, Oh J, Choi J H, Lee S C and Nam H S 2012 *Acta Mater.* **60** 4908
[35] Wang H, Hu T, Qin J Y and Zhang T 2012 *J. Appl. Phys.* **112** 073520
[36] Deng L, Hu W Y, Deng H Q and Xiao S F 2010 *J. Phys. Chem. C* **114** 11026
[37] Deng L, Hu W Y, Deng H Q, Xiao S F and Tang J F 2011 *J. Phys. Chem. C* **115** 11355
[38] Vitos L, Ruban A, Skriver H L and Kollár J 1998 *Surf. Sci.* **411** 186
[39] Abbaspour M, Akbarzadeh H and Lotfi S 2018 *J. Alloys Compd.* **764** 323
[40] Yang J Y, Hu W Y and Tang J F 2011 *Sci. China- Phys. Mech. Astron.* **54** 846
[41] Huang R, Wen Y H, Zhu Z Z and Sun S G 2012 *J. Phys. Chem. C* **116** 11837
[42] Yang J Y, Hu W Y and Tang J F 2015 *Thin Solid Films* **593** 137
[43] Mottet C, Rossi G, Baletto F and Ferrando R 2005 *Phys. Rev. Lett.* **95** 035501
[44] Feng D, Feng Y, Yuan S, Zhang X and Wang G 2017 *Appl. Therm. Eng.* **111** 1457
[45] Hamid I, Fang M and Duan H 2015 *AIP Adv.* **5** 047129
[46] Purja Pun G P and Mishin Y 2009 *Philos. Mag.* **89** 3245
[47] Müller M, Erhart P and Albe K 2007 *J. Phys.: Condens. Matter* **19** 326220
[48] Perdew J P, Wang Y and Engel E 1991 *Phys. Rev. Lett.* **66** 508
[49] Haftel M I, Andreadis T D, Lill J V and Eridon J M 1990 *Phys. Rev. B* **42** 11540
[50] Fu C, Ye Y, Yoo M and Ho K 1993 *Phys. Rev. B* **48** 6712
[51] Lee E and Lee B J 2010 *J. Phys.: Condens. Matter* **22** 175702
[52] Hendy S, Brown S A and Hyslop M 2003 *Phys. Rev. B* **68** 241403
[53] Raut J S, Bhagat R B and Fichthorn K A 1998 *Nanostruct. Mater.* **10** 837
[54] Yang J Y, Hu W Y, Wu Y Q and Dai X Y 2012 *Cryst. Growth Des.* **12** 2978